A miniaturized low power Pirani pressure sensor based on suspended graphene

Romijn, Joost; Vollebregt, Sten; Dolleman, Robin J.; Singh, Manvika; van der Zant, Herre S.J.; Steeneken, Peter; Sarro, Pasqualina

DOI
10.1109/NEMS.2018.8556902

Publication date
2018

Document Version
Final published version

Published in
Proceedings of the 13th Annual IEEE International Conference on Nano/Micro Engineered and Molecular Systems

Proceedings of the 13th Annual IEEE International
Conference on Nano/Micro Engineered and Molecular Systems
April 22-26, 2018, Singapore

A Miniaturized Low Power Pirani Pressure Sensor Based on Suspended Graphene

Joost Romijn*, Sten Vollebregt*, Robin J. Dolleman†, Manvika Singh*, Herre S.J. van der Zant†,
Peter G. Steeneken‡† and Pasqualina M. Sarro*
* Department of Microelectronics, Else Kooi Laboratory, Delft University of Technology, The Netherlands
† Department of Quantum Nanoscience, Kavli Institute of Nanoscience, Delft University of Technology, The Netherlands
‡ Department of Precision and Microsystems Engineering, Delft University of Technology, The Netherlands
Contacting author: s.vollebregt@tudelft.nl

***Abstract*—Worlds first graphene-based Pirani pressure sensor is presented. Due to the decreased area and low thickness, the graphene-based Pirani pressure sensor allows for low power applications down to 0.9 mW. Using an innovative, transfer-free process, suspended graphene beams are realized. This allows for up to 100x miniaturization of the pressure sensor area, while enabling wafer-scale fabrication. The response of the miniaturized pressure sensor is similar to that of the much larger state-of-the-art Si-based Pirani pressure sensors, demonstrating the potential of graphene-based Pirani sensors.**

I. Introduction

Pressure sensors are one of the most widely used MEMS devices integrated in various systems and circuits and are a vital member of the sensor family. They require constant improvement to facilitate more functionalities. Nowadays, the trend of miniaturization is still very active and recent years awakened a trend of reducing power consumption and device dimensions. These trends are also relevant for MEMS devices and in this case, pressure sensors.

Pirani pressure sensors are an attractive and often used pressure sensor architecture due to their simplicity and robustness as no hermetic cavity, moving parts or accurate deflection measurement methods are required. Current Pirani implementations have typical dimensions of 100 μm x 200 μm with a power consumption of $\sim$1 mW or more [2]–[4]. The sensitivity and pressure range of these devices is limited as the gap can not be reduced to the nm range. A scaling law for the required power and dimensions for equal power consumption is taken from a widely used and confirmed analytical model for Pirani pressure sensors [5]. Moreover, the defined ohmic heating of the conductive bridge material is given by Equation 1, where I_b is the electric current forced through the conductive bridge, R_0 the bridge resistance at ambient temperature and pressure, κ_b the bridge thermal conductivity and w, L and t the bridge width, length and thickness respectively. It is clear that smaller dimensions require less power to obtain similar ohmic heating. This is where graphene has a huge advantage, as it is only a few nm thick.

$$\delta = \frac{I_b^2 R_0}{\kappa_b w L t} \tag{1}$$

A nano Pirani pressure sensor based on a CNT implementation exists [1], but it does not have a selective fabrication process. In this research, world's first graphene-based Pirani pressure sensors with a selective fabrication process [6] are presented that are significantly smaller then current implementations and therefore consume less power. Furthermore, their sensitivity is comparable to current state-of-the art Pirani pressure sensors.

By using graphene as the conductive bridge material, the footprint of the Pirani pressure sensor could be reduced by a factor 100x compared to existing micro-Piranis [2]. This is beneficial for many applications, such as in situ pressure monitoring inside vacuum sealed cavities for MEMS devices.

Furthermore, graphene-based Pirani pressure sensors with tuned nano-gap sizes will allow operation at ambient pressures and could be used for applications such as barometers for altitude measurements, as the gap size determines the operation range [5].

II. Experimental

The main fabrication steps are illustrated in Fig. 1. The first step (Fig. 1a) starts with bare silicon (Si) on which thermal wet oxidation is performed to create a silicon dioxide (SiO_2) layer of 600 nm. This is followed by the sputter deposition of a 50 nm thick molybdenum (Mo) layer that functions as a catalyst in the graphene growth process. The Mo layer is patterned by dry etching through a photoresist mask in a chlorine and hydrogen bromide gas mixture (Cl/HBr). The photoresist mask is stripped in n-methylpyrrolidon (NMP) at 70°C, since conventional organic cleaning involves nitric acid (HNO_3) which etches Mo.

In the second step (Fig. 1b), graphene is deposited by chemical vapor deposition (CVD) at 915 °C for 20 minutes. The carbon source is methane (CH_4), which reacts at the Mo surface so that carbon solutes in the Mo. During cooling the carbon solubility of Mo drops, which selectively forms multilayer graphene of $\sim$8 nm thick on its surface [7].

In the next step (Fig. 1c), metal interconnect is deposited by a lift-off process using evaporated gold/chromium (Cr/Au) as this material provides a good contact resistance to the multilayer graphene. This is followed by the cavity formation. The graphene/Mo stack is suspended by selectively removing the SiO_2 layer in a buffered hydrofluoric acid (BHF) wet etch. By controlling the cavity depth through the oxide thickness, the pressure range of the Pirani pressure sensor can be tuned.

978-1-5386-5273-2/18/$31.00 © 2018 IEEE

In the final step (Fig. 1d), the Mo layer is removed by wet etching in hydrogen peroxide (H_2O_2). After critical point drying (CPD), the graphene adheres to the SiO_2 creating the heater bridge over the cavity. The absence of any graphene transfer steps combined with selective CVD graphene deposition enables wafer-scale fabrication of new devices with high yield [6].

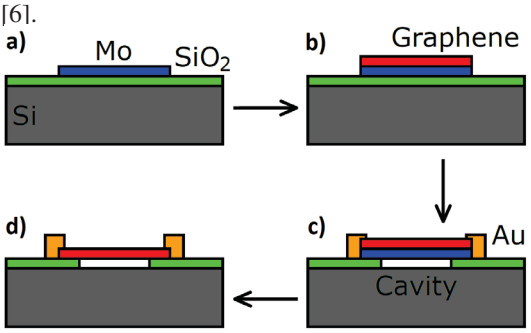

Fig. 1. Fabrication process overview of the suspended graphene pressure sensor [6] consisting of; a) deposition and patterning of 50 nm Mo on a 600 nm SiO_2 layer; b) selective CVD of graphene on Mo; c) 100 nm Au/Cr contact deposition and wet etching of the cavity using a photoresist mask; d) wet etching of Mo and CPD, resulting in a suspended graphene Pirani pressure sensor.

III. Results and Discussion

Scanning electron microscope (SEM) images in Fig. 2 show suspended ∼8 nm thick multilayer graphene bridge used in the Pirani pressure sensor. Different aspect ratios L/w up to 8 have been realized. High aspect ratios allow either higher sensitivity or lower power consumption. The devices are upto 100x smaller in area than current implementations [2].

The wet SiO_2 etching of the cavity under the graphene bridge does not result in straight cavity sidewalls. This influences the effective length of the bridge and is more dominant for the aspect ratio L/w = 6/5 presented in Fig. 2b. The aspect ratio of L/w = 8 in Fig. 2a shows a bridge that significantly sags towards the substrate. For aspect ratios above L/w = 8 the graphene bridges came in contact with the substrate. The graphene forms on the rough catalyst surface. As a consequence, the graphene is corrugated after removal of the Mo and extension of these corrugations could cause the graphene bridge to be larger than the gap and result in the observed sagging of the bridge. This effect could reduce the effective gap distance between the graphene bridge and the silicon substrate.

No visual damage to the graphene bridges due to processing is observed. Raman spectroscopy is performed during three stages of the process to investigate this further. The results in Fig. 3 show identical D/G peak ratios before and after release, which indicates no change in defect density [8], [9]. This provides evidence that the processing does not affect the graphene quality.

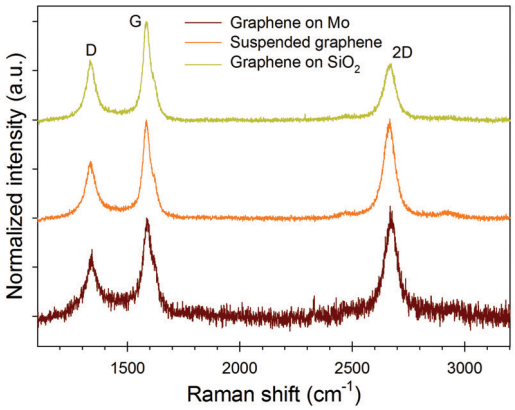

Fig. 3. Raman spectroscopy of graphene strips at three stages of the process. Including before release on Mo, after release on SiO_2 and suspended. Identical D/G ratios indicate no change in defect density. A Renishaw inVia Raman spectroscope with a red 633 nm laser is used.

The sensitivity of the Pirani pressure sensor is related to the gap depth. In the presented fabrication process, the gap depth can be varied by changing the thickness of the SiO_2. Furthermore, the sagging bridge is an disadvantageous result when attempting to control the gap depth. Careful control over the process is necessary to guarantee a reproducible and high yield fabrication.

A. Thermal Coefficient of Resistance

The sensitivity of the Pirani pressure sensor depends on the TCR of the heater material. The TCR of non-suspended graphene was determined by heating a sample on a temperature controlled chuck in a probe station to different temperatures while measuring its electrical resistance. The electrical resistance measurements are done at low bias voltage conditions to minimize the effect of resistive self-heating.

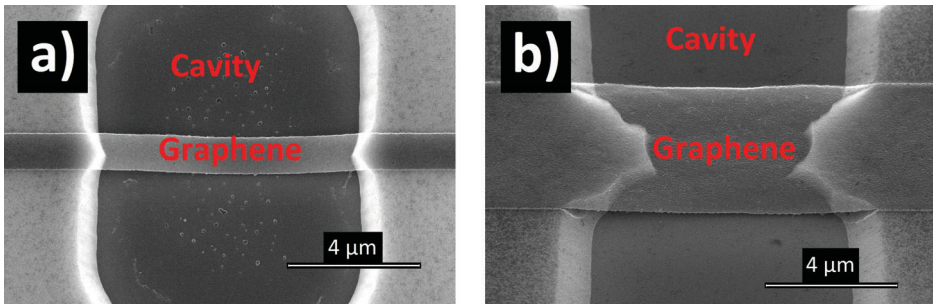

Fig. 2. SEM images of suspended graphene bridges, a) high aspect ratio (width of 1 μm and length of ∼8 μm) and b) low aspect ratio (width of 5 μm and length of ∼6 μm). Images taken under a 45° angle. The devices were visualized through a FEI XL50 SEM.

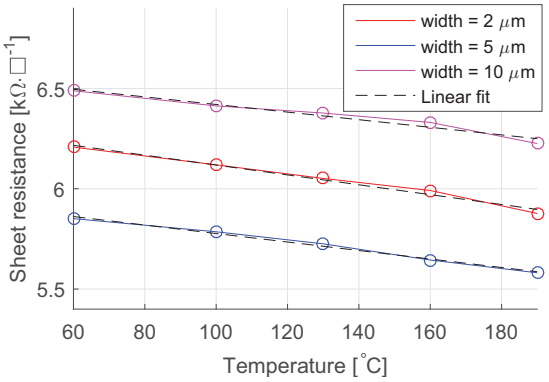

Fig. 4. Sheet resistance measurement results of non-suspended graphene strips 206 μm long and with different widths at different chuck temperatures. The difference in sheet resistance between the different strip widths is ~5% and is considered due to process variations. The figure includes linear fits of which the largest fit error is 0.5%.

In Fig. 4 the results of non-suspended graphene strips of different widths are depicted. The TCR is constant over this temperature range. An average of (-3.6 $\pm$ 0.5) $\cdot 10^{-4}$ K^{-1} is found for the graphene strip, which matches values reported in literature [10].

B. Pressure Dependency

The pressure dependency of the electrical resistance of suspended and non-suspended graphene-based Pirani pressure sensors was investigated. The samples were placed in a pressure controlled vacuum chamber. The experimental setup is depicted in Fig. 5. The source and measurement unit (SMU) and pump controller are perform the measurements and drive the pressure controller, which sets the pressure in the vacuum chamber using a nitrogen (N_2) gas source. The SMU performs 4-wire current and voltage measurements on the sample.

The pressure controller was set to the desired value and reaches a stable pressure before measuring the resistance. A bias voltage sweep that incorporates both positive and negative voltage values, is performed by the SMU. The sample remains biased during pressure adjustments to reduce possible variations in temperature of the graphene pressure sensor. An upward and downward pressure sweep is performed to monitor drift and hysteresis of the resistance. Neither was observed in the reported measurement results.

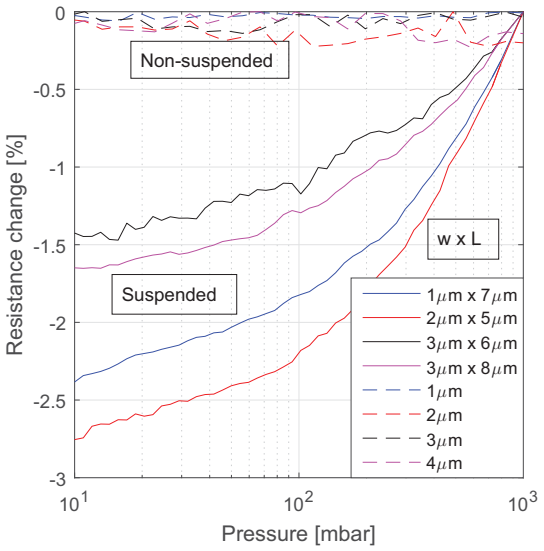

Fig. 6. Resistance pressure dependency of suspended and non-suspended graphene strips, marked in solid and dashed lines respectively, with different geometries, biased at 7.5 V. Total graphene strip length is 20 μm. Average sheet resistance is 830 Ω.

$$\Delta R = \frac{R(p) - max(R(p))}{max(R(p)} * 100 \qquad (2)$$

The resistance measurement results of suspended and non-suspended devices with different aspect ratios at different pressures are depicted in Fig. 6 as defined in Equation 2. Note that these devices have a significantly lower sheet resistance than the sample used to determine the TCR. A clear pressure dependence of the resistance is observed for the suspended devices, while the non-suspended devices show no measurable change. The maximum change in resistance is typically observed for narrow devices, which are thus more sensitive. However, a direct quantitative model for the relation between device geometry and resistance change is not derived.

The largest measured maximum resistance change (in Fig. 6) of the devices is approximately -2.75% at a power consumption of 8.5 mW. This maximum change is higher than that of

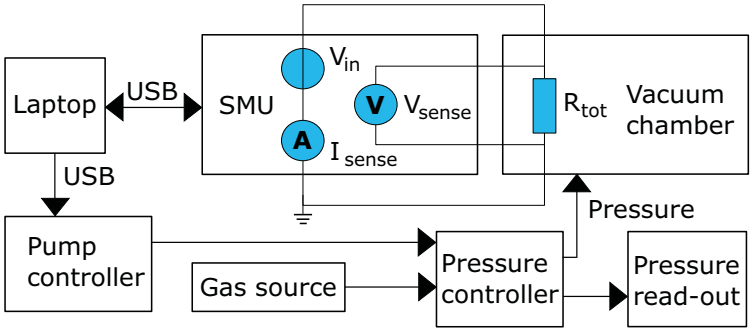

Fig. 5. Schematic illustration of the automatic pressure dependency measurements. A Keysight B2901A SMU, Rigol DP832A voltage source pump controller, Proportionair PA2254 dual-valve pressure controller and Keithey 199 pump readout are used in the experimental setup.

traditional Piranis found in literature with comparable power consumption [11]. Therefore, these graphene-based Pirani pressure sensors provide an improved performance compared to state-of-the-art implementations using other materials.

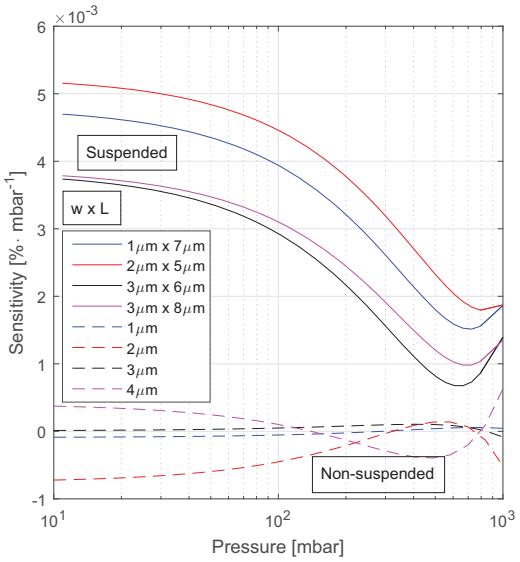

Fig. 7. Sensitivity of suspended and non-suspended graphene strips, marked in solid and dashed lines respectively. Different geometries biased at 7.5 V and total graphene strip length of 20 μm. Average sheet resistance is 830 Ω.

The sensitivity of the responses depicted in Fig. 6 is calculated by fitting a third order polynomial to the measurement data and taking the derivative. The results are given in Fig. 7. The non-suspended devices show a negligible sensitivity compared to the suspended devices. The maximum sensitivity for all suspended devices is measured at 10 mbar or lower. The sensitivity appears to rise again around ambient pressure, but this is an artifact caused by the third order polynomial fit.

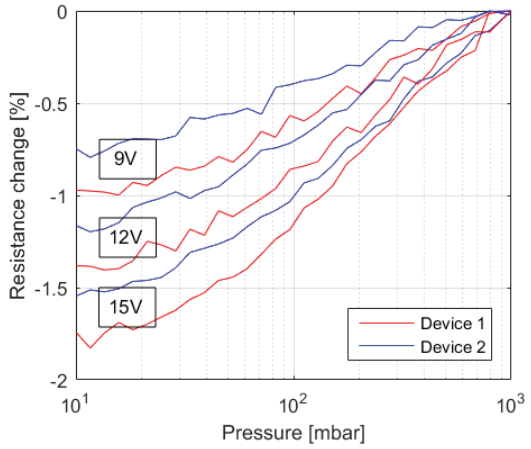

Fig. 8. Resistance pressure dependency of two suspended graphene strips with equal geometry and different bias conditions. The average sheet resistance is 10.6 kΩ due to more defects and the graphene strips are 5 μm wide and $\sim$7 μm long with a total strip length of 42 μm.

Another batch of graphene-based Pirani pressure sensors was fabricated which incorporates graphene with a higher sheet resistance (a factor of $\sim$13x) compared to the first batch. A single geometry is measured in this batch, with an aspect ratio of $\sim$1.4 that corresponds best with the geometry 3μm x 6μm of the first batch. The pressure dependent resistance change measurement results of this batch are depicted in Fig. 8. The devices biased at 9 V have a power consumption of 0.9 mW, which is a reduction with a factor of $\sim$9x compared to the first batch. In contrast, the maximum resistance change is reduced by a factor of $\sim$1.5x. These results indicate that graphene with more defects is favored for low power applications.

IV. Conclusions

We have demonstrated the feasibility of fabricating high-sensitivity graphene Pirani pressure sensors by a wafer-scale fabrication process. The fabrication process does not influence graphene quality. The TCR of the implemented multilayer graphene was found to be of the same order as reported in literature. Devices have been reduced by 100x compared to current implementations. The electrical resistance of suspended graphene bridges showed a pressure dependency, compared to a negligible pressure dependency for non-suspended graphene strips. A maximum resistance change of -2.75% was achieved, which is higher compared to traditional Pirani pressure sensors. A low power consumption of 0.9 mW was achieved while only reducing the sensitivity by a factor $\sim$1.5x. The excellent device performance, high volume wafer-scale fabrication process and the potential of tuning the device gap enable a wide range of future applications for suspended graphene-based Pirani pressure sensors.

Acknowledgment

The authors would like to thank the Delft University of Technology Else Kooi Lab staff for processing support. This work is partially funded by the Netherlands Organisation for Scientific Research (NWO) with project numbers 13307 and 13319 and the European Union's Horizon 2020 research and innovation programme under grant agreement number 649953.

References

[1] F. Yu and J. Zhang, *IEEE Transactions on Nanotechnology*, vol 12, p.p. 323-329, 2013.
[2] M. Piotto et al, *Procedia Engineering*, vol 168, p.p. 766-769, 2016.
[3] M. Piotto et al, *Sensors and Actuators*, vol 263, p.p. 718-726, 2017.
[4] F. Santagata et al, *Journal of Microelectromechanical Systems*, vol 20, p.p. 676-684, 2011.
[5] K. Khosraviani and A.M. Leung, *Journal of Micromechanics and Microengineering*, vol 19, 045007, 2009.
[6] S. Vollebregt et al, *Proc. of Micro Electro Mechanical Systems (MEMS) conference*, p.p. 17-19, 2016.
[7] Y. Wu et al, *Carbon*, vol 50, issue 14, p.p. 5226-5231, 2012.
[8] S. Vollebregt et al, *Carbon*, vol 50, issue 10, p.p. 3542-3554, 2012.
[9] L.G. Cançado et al, *Nano Letters*, vol 11, no 8, p.p. 3190-3196, 2011.
[10] J.J. Bae et al, *Current Applied Physics*, vol 16, no 9, p.p. 1236-1241, 2010.
[11] J. Claudel et al, *Procedia Engineering*, vol 168, p.p. 798-801, 2016.